ISSN 1070-3284, Russian Journal of Coordination Chemistry, 2020, Vol. 46, No. 1, pp. 64–73. © Pleiades Publishing, Ltd., 2020.

Syntheses, Crystal Structures, and Properties of Ferrocene–Carboxylate Coordination Complexes through Modulating the Auxiliary Ligands

R. Y. Li[a], Y. J. Li[a], X. H. Lu[a], Y. T. Zhang[b], X. L. Gao[a], X. T. Wang[a], Z. G. Li[a], Y. Zhu[a], and J. P. Li[a, *, **]

[a]*College of Chemistry and Molecular Engineering, Zhengzhou University, Henan, 450052 P.R. China*

[b]*High Middle School no. 47 , Zhengzhou, 450000 P.R. China*

**e-mail: ljp-zd@zzu.edu.cn*

***e-mail: ljp-zd@163.com*

Received October 23, 2018

Abstract—Self-assemblies of the flexible ferrocenyl block (3-carboxy-1-oxopropyl)-ferrocene with Zn(II)/Cd(II) cations in the presence of different N-containing auxiliary ligands have led to four coordination complexes, namely, $[\{Zn(FcCOC_2H_4COO)_2(Pbbbm)\}_2] \cdot 1/2CH_3OH$ (**I**), $[\{Zn\text{-}(FcCOC_2H_4COO)_2(Btx)\}_2] \cdot 2H_2O$ (**II**), $[Zn(FcCOC_2H_4COO)_2(Bbbmd)]$ (**III**), and $[Cd(\eta^2\text{-}FcCOC_2H_4COO)_2(Bbbmd)]$ (**IV**) (Fc = $(\eta^5\text{-}C_5H_4)Fe(\eta^5\text{-}C_5H_4)$, Pbbbm = 1,4-bis(benzimidazol-1-ylmethyl)-benzene, Btx = 1,4-bis(1,2,4-triazol-1-ylmethyl)-benzene, Bbbmd = bis-(1-benzimidazolymethylene)-(2,5-thiadiazoly)-disulfide). Their structures have been determined by single-crystal X-ray diffraction analyses (CIF files CCDC nos. 948969 (**I**), 948970 (**II**), 948971 (**III**), 948972 (**IV**)), and further characterized by elemental analyses, IR spectra, and thermogravimetric analyses. Crystallographic characterization shows the two neutral complexes **I** and **II** to have dinuclear structures which are bridged through Pbbbm and btx, while complexes **III** and **IV** give mononuclear structures. The four complexes exhibit some differences in their conformations, which can be attributed to the influence of auxiliary ligands. Notably, various weak interactions are discovered in **I**–**IV**, and they have significant contributions to self-assembly, which extend the two dimers or mononuclear complexes to infinite 3D supramolecular networks. The electrochemical studies of **I**–**IV** in DMF solution display irreversible redox waves and they all show single peaks in correspondence with redox processes of Fe(II)/Fe(III) couple electron-transfer process of ferrocenyl moieties.

Keywords: crystal structure, π···π interaction, electrochemistry, ferrocenyl carboxylate

DOI: 10.1134/S1070328420010042

INTRODUCTION

In past decades, the design and synthesis of metal-organic complexes have become an active area of crystal engineering and supramolecular chemistry, not only for their intriguing architectures and topologies, but also for their tailor-made applications in catalysis, magnetism, and nonlinear optics [1–5]. These metal-organic complexes can be constructed by coordination or/and hydrogen bonds or other weaker interactions, such as π···π stacking interactions. The key factors contributing to the self-assembly of coordination complexes with unique structures and functions are the elaborately selected organic ligands, the coordination geometry of metal ions, metal-ligand ratio, and the pH value of the solution. In this field, aromatic ferrocene has captivated much attention of chemists owing to its relatively better stereochemical and electrochemical properties [6]. So far, large quantities of organic ligands containing ferrocene unit have been extensively used as building blocks for forming metal-organic coordination complexes [7–10]. In addition, many researches have proven that the ligands which contain carboxylate groups are good candidates for the synthesis of metal-organic complexes with novel structure types [11–13], which is due to their strong coordination capability and various coordination modes of carboxylate groups. Therefore, the strategy of attaching ferrocenyl carboxylates ligands facilitates the formation of metal-organic complexes with peculiar features. Furthermore, the introduction of a second organic ligand to such synthetic systems has been found to be a very effective route for modifying the structures and properties of the final products. Among various organic ligands, neutral flexible nitrogen-heterocyclic ligands with the π-conjugated character exhibit the outstanding function as auxiliary ligands, because they may form strong π···π stacking interactions and further lead to variable π–π interactions modes and architectures [14, 15]. The synthesis of π-stacked molecular architectures is of great impor-

tance to understand the electronic interactions between molecules since π···π interactions are essential in biology and the functions of organic semiconducting materials [16–18].

According to above considerations and as an extension of our earlier studies [19], in this paper, by employing (3-carboxy-1-oxopropyl)-ferrocene as the major ligand and a series of organic nitrogen-heterocyclic ligands (Scheme 1) as the second metal linker, we have successfully obtained four Zn(II) and Cd(II) complexes (Scheme 2). Herein, the report is on syntheses, crystal structures, electrochemical and thermal properties of the four complexes—$[\{Zn(FcCOC_2H_4COO)_2(Pbbbm)\}_2] \cdot 1/2CH_3OH$ (**I**), $[\{Zn(FcCOC_2H_4COO)_2(Btx)\}_2] \cdot 2H_2O$ (**II**), $[Zn(FcCOC_2H_4COO)_2(Bbbmd)]$ (**III**), and $[Cd(\eta^2\text{-}FcCOC_2H_4COO)_2(Bbbmd)]$ (**IV**) (Fc = $(\eta^5\text{-}C_5H_4)Fe(\eta^5\text{-}C_5H_4)$, Pbbbm = 1,4-bis(benzimidazol-1-ylmethyl)-benzene, Btx = 1,4-bis(1,2,4-triazol-1-ylmethyl)-benzene, Bbbmd = bis-(1-benzimidazolymethylene)-(2,5-thiadiazoly)-disulfide). There is also the detailed discussion on various weak stacking interactions in **I**–**IV**.

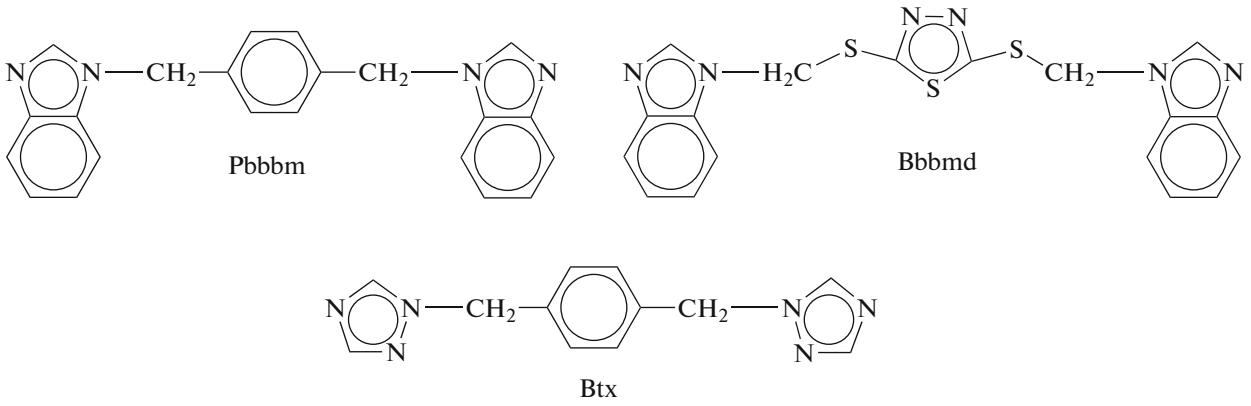

Scheme 1.

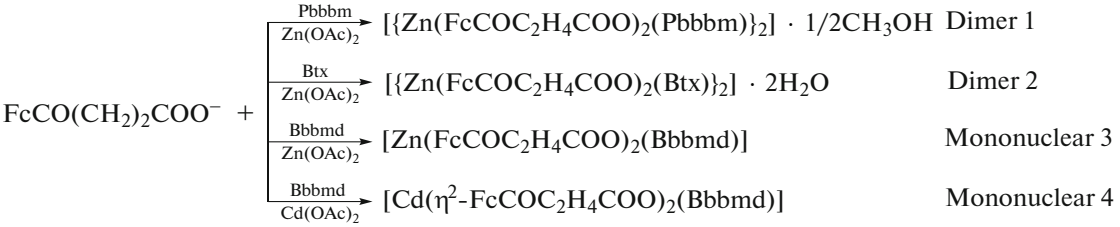

Scheme 2.

EXPERIMENTAL

Materials and methods. We prepared (3-carboxy-1-oxopropyl)-ferrocene and corresponding sodium salt according to literature methods [20], Pbbbm, Btx, and Bbbmd according to the literature [21]. All other chemicals were obtained from commercial sources and used without further purification. The analysis of carbon, hydrogen and nitrogen was conducted on a FLASH EA 1112 elemental analyzer. IR spectra were taken on a BRUKER TENSOR 27 spectrophotometer with KBr pellets in 400–4000 cm^{-1} region. Thermogravimetry (TG) and differential scanning calorimetry (DSC) measurements were performed by heating samples of **I**–**IV** from 30–750°C at a rate of 10°C/min in air on a NETZSCH STA 409PC differential thermal analyzer. Cyclic voltammetric experiments were

performed by employing a CHI 660B electrochemical analyzer. There was a three-electrode system composed of a platinum working electrode, a platinum wire auxiliary electrode, and an Ag/AgCl reference electrode. The measurements were conducted in DMF solutions with the tetrabutyl ammonium perchlorate (n-Bu_4NClO_4) (0.1 mol dm^{-3}) as supporting electrolyte. The working electrode was polished to prevent fouling. Pure N_2 gas bubbled through the electrolytic solution was to remove oxygen.

Synthesis complex I. The methanol solution (5 mL) of adjuvant ligand Pbbbm (16.4 mg, 0.05 mmol) was added to a methanol solution (3 mL) of $Zn(OAc)_2 \cdot 2H_2O$ (11.0 mg, 0.05 mmol), and then the methanol solution (4 mL) of $FcCOC_2H_4COONa$ (30.8 mg, 0.10 mmol) was added to above mixture. The mixture was stirred and then filtered. The final mixture was kept in the dark at room temperature. One week later, good quality red crystals stable in the air were obtained from the resultant red solution. The yield was 57%.

For $C_{100}H_{88}N_8O_{12}Zn_2Fe_4$

Anal. calcd., %	C, 61.40	H, 4.58	N, 5.70
Found, %	C, 61.16	H, 4.71	N, 5.75

IR spectrum (KBr; ν, cm^{-1}): 3441s, 3109 s, 1662 s, 1601s, 1516 s, 1453 m, 1393 s, 1335 w, 1207 m, 1188 m, 1011 w, 822 s, 745 s, 485 m.

Synthesis complex II was carried by the similar procedure to that described for **I** except using Btx (0.05 mmol) for **II** instead of Pbbbm. Two weeks later, good quality red crystals were obtained from the resultant red solution. The yield was 48%.

For $C_{80}H_{76}N_{12}O_{12}Zn_2Fe_4$

Anal. calcd., %	C, 53.75	H, 4.51	N, 9.40
Found, %	C, 53.68	H, 4.41	N, 9.63

IR spectrum (KBr; ν, cm^{-1}): 3550 m, 3442 m, 1660 s, 1602 s, 1503 m, 1414 s, 1130 m, 1081 w, 1003 w, 872 w, 776 w, 485 m.

Synthesis complex III was carried by the similar procedure to that for **I**, and then Bbbmd was used to replace Pbbbm. Approximately two weeks later, good quality red crystals were obtained from the resultant red solution. The red crystals were also stable in the air. The yield was 45%.

For $C_{46}H_{40}N_6O_6S_3ZnFe_2$

Anal. calcd., %	C, 52.77	H, 3.82	N, 8.03
Found, %	C, 52.48	H, 3.71	N, 7.95

IR spectrum (KBr; ν, cm^{-1}): 3428 s, 1710 s, 1651 s, 1615 s, 1384 m, 1086 m, 877 w, 748 w, 532 w, 494 w.

Synthesis complex IV was carried by the similar procedure to that for **III**, and $Cd(OAc)_2 \cdot 2H_2O$ was used to replace $Zn(OAc)_2 \cdot 2H_2O$. Three weeks later, good quality red crystals were obtained from the resultant red solution. The yield was 51%.

For $C_{46}H_{40}N_6O_6S_3CdFe_2$

Anal. calcd., %	C, 50.50	H, 3.66	N, 7.68
Found, %	C, 50.18	H, 3.71	N, 7.89

IR spectrum (KBr; ν, cm^{-1}): 3437 m, 3103 m, 1664 s, 1553 s, 1507 m, 1495 s, 1390 s, 1259 m, 1087 w, 1027 w, 1004 w, 882 w, 747 s, 487 m.

X-ray crystallography. The diffraction intensity data of **I**–**IV** were collected by a Rigaku RAXIS-IV and SATURN-724 imaging plate area detector with graphite monochromated MoK_α radiation (λ = 0.71073 Å) at 293(2) K temperature. The structures were solved by direct methods and expanded with Fourier techniques. The non-hydrogen atoms were refined anisotropically. Hydrogen atoms were included but not refined. The final cycle of full-matrix least-squares refinement was based on observed reflections and variable parameters. All calculations were performed by using SHELX-2014 crystallographic software package [22]. The data of **I** and **II** were corrected with SQUEEZE to remove the solvent molecules due to severe crystallographic disorder [23]. Table 1 showed crystallographic crystal data and processing parameters for complexes **I**–**IV** and Table 2 listed corresponding selected bond lengths and bond angles.

Supplementary crystallographic material for structures has been deposited with the Cambridge Crystallographic Data Centre (CCDC nos. 948969 (**I**), 948970 (**II**), 948971 (**III**), 948972 (**IV**); deposit@ccdc.cam.ac.uk or www.ccdc.cam.ac.uk/data-request/cif).

RESULTS AND DISCUSSION

The X-ray diffraction analysis reveals that **I** and **II** have the same structure. Herein, we only described the structure of **I** in detail. Crystallographic analysis reveals that **I** exhibits a symmetric dinuclear structure which is situated on an inversion center (Fig. 1). The Zn(II) metal center is in tetrahedron coordination linked by two carboxylate oxygen donors together with two Pbbbm nitrogen donors. Each carboxyl group from $FcCOC_2H_4COO^-$ ligand donates one oxygen atom to Zn(II) metal center. The two symmetry-

Table 1. Crystallographic data and structure refinement for complexes **I**–**IV**

Parameter	Value			
	I	**II**	**III**	**IV**
Fw	1947.92	1751.71	1046.09	1093.16
Crystal system	Triclinic	Triclinic	Triclinic	Triclinic
Space group	$P\bar{1}$	$P\bar{1}$	$P\bar{1}$	$P\bar{1}$
a, Å	13.074(3)	12.832(3)	12.309(3)	12.453(3)
b, Å	13.941(3)	13.335(3)	13.023(3)	13.227(3)
c, Å	14.300(3)	14.138(3)	15.891(3)	15.889(3)
α, deg	89.82(3)	82.85(3)	113.75(3)	66.38(3)
β, deg	65.41(3)	66.93(3)	104.92(3)	67.18(3)
γ, deg	74.67(3)	62.72(3)	98.12(3)	81.82(3)
V, Å^3	2268.7(8)	1973.7(8)	2164.9(8)	2210.0(8)
Z	1	1	2	2
ρ_{calcd}, g cm^{-3}	1.209	1.474	1.605	1.643
F(000)	1004	900	1072	1108
θ Range for data, deg	3.05–27.46	2.25–25	3.16–25.00	2.43– 27.52
Reflections collected/unique	27647/10317	20181/6940	21819/7586	26934/10074
Data/restraints/parameters	10317/0/568	6940/40/496	7586/1/577	10074/0/617
Goodness-of-fit	1.050	1.109	1.074	1.110
Final R_1*, wR_2**	0.0518, 0.1040	0.0573, 0.1058	0.0375, 0.0964	0.0401, 0.0806

* $R_1 = ||F_o| - |F_c||/|F_o|$. ** $wR_2 = [w(|F_o^2| - |F_c^2|)^2/w|F_o^2|^2]^{1/2}$.

related Pbbbm groups, exhibiting two benzimidazole rings at one side of the benzene ring with dihedral angles of 78° or 105.6° between benzene rings and benzimidazole rings, bridges Zn(II) metal centers via two benzimidazole nitrogen atoms, which results in the dinuclear structure. The Zn···Zn separation is 11.157(4) Å in **I** which is slightly longer than the corresponding value for **II** (11.084(4) Å). The Zn–O/N bond lengths in **I** and **II** are consistent with the reported tetrahedral Zn(II) complexes [24–26]. Some main angles around Zn(II) in **I** and **II** range from 102.79(13)° to 112.77(14)°, which are slightly deviate from idealized tetrahedron geometry. It is worthy to note that there are the weak intramolecular C–H···O hydrogen bonds (Å) in **I** and **II** (Figs. 1a, 1b, right). The H···O distances (bond angles) of the hydrogen bonds in **I** are 2.47 Å (137°) for C(43*A*)H(43*A*)···O(4*A*), 2.34 Å (158°) for C(8*A*)H(8*A*)···O(5*A*), 2.28 Å (131°) for C(36*A*)H(36*A*)···O(5*A*) and 2.49 Å (103°) for C(26*A*)H(26*A*)···O(2*A*), while in **II**, the H···O distances (bond angles) of the hydrogen bonds are 2.54 Å (121°) for C(30)H(30*A*)···O(2), 2.47 Å (122°) for C(40*A*)H(40*B*)···O(2), 2.54 Å (153°) for C(19*A*)H(19*B*)···O(5) and 2.36 Å (129°) for C(29)H(29*A*)···O(5), which are all shorter than some C–H···O hydrogen bonds reported in some literature [27, 28], and they play a crucial role in forming such conformation of dinuclear Zn(II) complexes. Analysis of the crystal packing (Fig. 2) reveals that the dinuclear structure of **I** is further extended to 2D layers by the intermolecular C(15*A*)H(15*A*)···O(2*A*) hydrogen bonds (H···O distances: 2.47 Å, bond angles: 167°). While in **II**, the intermolecular O(7)H(2*w*)···O(3),

Table 2. Selected bond lengths (Å) and bond angles (deg) for complexes **I**–**IV***

Bond	*d*, Å	Bond	*d*, Å
		I	
Zn(1)–O(3)	1.950(3)	Zn(1)–O(6)	1.975(3)
Zn(1)–N(2)	2.053(3)	Zn(1)–N(3)	2.013(3)
		II	
Zn(1)–O(4)	1.981(3)	Zn(1)–O(1)	1.983(3)
Zn(1)–N(1)	2.013(3)	Zn(1)–N(6)$^{\#1}$	2.018(4)
		III	
N(4)–Zn(1)	2.054(2)	N(6)–Zn(1)	2.068(2)
O(4)–Zn(1)	2.018(2)	O(1)–Zn(1)	1.952(2)
		IV	
Cd(1)–O(8)	2.264(8)	Cd(1)–O(11)	2.347(8)
Cd(1)–O(10)	2.347(8)	Cd(1)–N(7)	2.314(8)
Cd(1)–N(12)	2.263(8)	Cd(1)–O(9)	2.401(8)
Angle	ω, deg	Angle	ω, deg
		I	
O(3)Zn(1)O(6)	110.65(3)	O(3)Zn(1)N(3)	111.91(13)
O(6)Zn(1)N(3)	118.71(13)	O(3)Zn(1)N(2)	96.64(13)
O(6)Zn(1)N(2)	103.67(13)	N(3)Zn(1)N(2)	112.77(14)
		II	
O(4)Zn(1)O(1)	102.79(13)	N(1)Zn(1)O(2)	85.45 (13)
O(4)Zn(1)N(6)$^{\#1}$	109.68(14)	O(1)Zn(1)O(2)	54.90(12)
O(4)Zn(1)O(2)	156.79(11)	O(1)Zn(1)N(6)$^{\#1}$	100.50(15)
O(4)Zn(1)N(1)	110.71(14)	N(1)Zn(1)N(6)$^{\#1}$	122.16(14)
O(1)Zn(1)N(1)	109.62(14)		
		III	
O(1)Zn(1)O(4)	141.67(9)	O(1)Zn(1)N(4)	97.14(10)
O(4)Zn(1)N(4)	108.09(10)	O(1)Zn(1)N(6)	101.42(9)
N(4)Zn(1)N(6)	98.06(9)	O(4)Zn(1)N(6)	102.99(10)
		IV	
O(8)Cd(1)N(12)	86.8(3)	N(7)Cd(1)O(9)	90.9(3)
N(12)Cd(1)O(10)	97.5(3)	N(12)Cd(1)N(7)	92.7(3)
O(8)Cd(1)N(7)	95.9(3)	O(8)Cd(1)O(9)	55.3(3)

* Symmetry transformations used to generate equivalent atoms: $^{\#1}$ $-x, -y, -z + 1$ (**I**); $^{\#1}$ $-x + 1, -y + 2, -z$ (**II**).

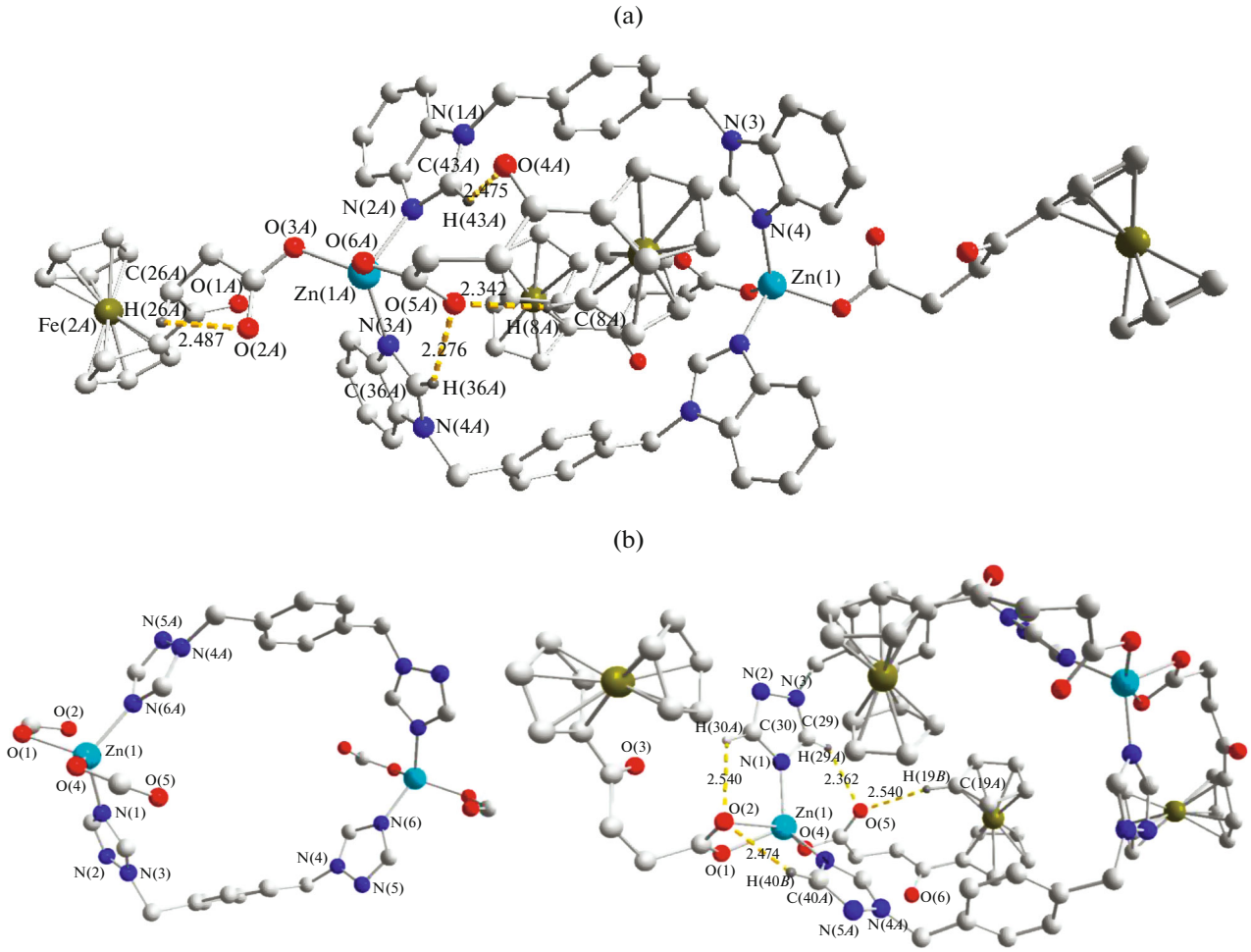

Fig. 1. The dinuclear structure of **I** (a) and **II** (b). Notice the weak C–H···O hydrogen bonds (Å). Hydrogen atoms are omitted for clarity in Fig. 1b (right).

O(7)H(1*w*)···O(5), C(34)H(34*A*)···O(7) and C(6)H-(6*A*)···O(7) hydrogen bonds between the dinuclear units and the crystallization water molecules are also observed, which also result in the two-dimensional layers. Through numerous weak C–H···O interactions in **I** and **II**, the non-coordinated methanol molecules are stabilized in the middle of the above-mentioned dinuclear units (Fig. 2). In addition, there are the intramolecular edge-to-face CH/π interactions 2.81 Å (dihedral angle: 80.1°; H/π-plane separation: 2.77 Å) for **I** between ferrocene rings and benzene rings of Pbbbm and 2.85 Å (dihedral angle: 81.2º; H/π-plane separation: 2.79 Å) for **II** between adjacent ferrocene rings and benzene rings of Btx. Additionally, the edge-to-face CH/π interactions between two intermolecular ferrocene rings with distance of 2.85 Å (dihedral angel: 80.6°; H/π-plane separation: 2.79 Å) for **I** and 2.86 Å (dihedral angel: 78.0°; H/π-plane separation: 2.73 Å) for **II**. The intramolecular and intermolecular weak interactions between aromatic rings offer further stability effect for solid-state structure of **I** and **II** and make separate dinuclear molecules to be interconnected to produce a 3D supramolecular structure (Fig. 2).

The X-ray diffraction analysis reveals both complexes **III** and **IV** exhibit similar mononuclear structures. Crystallographic analysis of complex **III** reveals that each mononuclear unit is compose of one Zn(II) metal center, two $FcCOC_2H_4COO^-$ anions and one chelate Bbbmd ligand. To the best of our knowledge, the metal-based supramolecular complexes constructed by the Bbbmd ligand are still very scarcely reported in the coordination polymers. According to Fig. 3a, Zn(II) metal center is coordinated by two oxygen atoms (O(1), O(4)), belonging to two

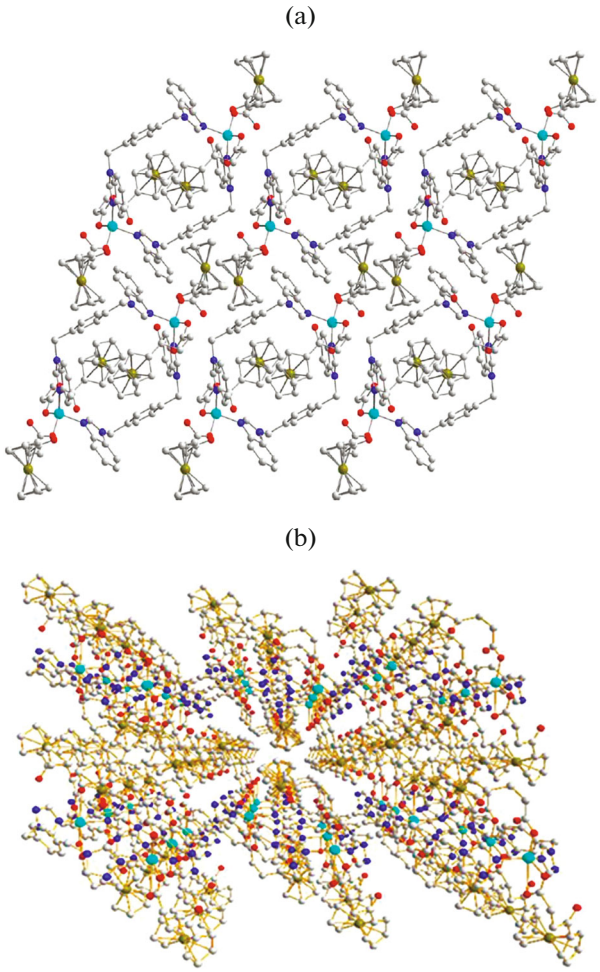

Fig. 2. The packed structure of **I** (a) and **II** (b).

$FcCOC_2H_4COO^-$ anions, and two nitrogen atoms (N(4), N(6)) from two different Bbbmd groups, which produces a distorted tetrahedral geometry. Different to complex **III**, it is noteworthy that Cd(II) metal center lies in a distorted octahedral coordination sphere defined by four oxygen atoms from two bidentate-chelating η^2-$OOCH_4C_2OCFc$ groups and two nitrogen atoms from one chelate Bbbmd ligand (Fig. 3b). Due to the difference in ionic radius of Zn(II) and Cd(II) metal centers, each $FcCOC_2H_4COO^-$ ligand in **III** and **IV**, respectively, adopts monodentate and bidentate coordination modes (Fig. 3). The Bbbmd in **III** (or **IV**) acts as a diconnector linking to Zn(II) (or Cd(II)) metal center to form a bowl-like structure. Lengths of the Zn–N/O bonds are all in the normal range [24–26]. In **IV**, Cd–N/O bond distances are similar to those of other Cd(II) complexes having a distorted octahedral environment, such as $[Cd(\eta^2\text{-}FcCOC_2H_4COO)_2(Pbbbm)]_2$, $Cd(\eta^2\text{-}FcCOC_2H_4COO)(Pbbbm)Cl]_2$ and etc. [19]. Compared with **I**–**III**, $FcCOC_2H_4COO^-$ ligands in **IV** adopt bidentate-chelating η^2-$OOCH_4C_2OCFc$ coordination mode, which is consistent with some foregoing Cd(II)-containing coordination complexes [19].

For **III** and **IV**, there are similar aromatic ring systems to that in **I**, so various π–π stacking interactions can be considered to exist. As seen from Fig. 3c, the center-to-center separations between two adjacent benzimidazole rings are 3.57 Å (**III**) and 3.45 Å (**IV**) [29, 30], indicating significant π···π interactions, and cause an infinite 2D layer. These 2D layers are further connected to 3D supramolecular networks by the following edge-to-face CH/π interactions: one is 2.72 Å (**III**) (2.68 Å for **IV**) (dihedral angel: 79.7° (**III**) (84.3° for **IV**); H/π-plane separation: 2.65 Å (**III**) (2.63 Å for **IV**)) between intermolecular ferrocene rings; the other is 2.81 Å (**III**) (2.89 Å for **IV**) (dihedral angel 86° (**III**) (99.5° for **IV**); H/π-plane separation: 2.78 Å (**III**) (2.78 Å for **IV**)) between intermolecular

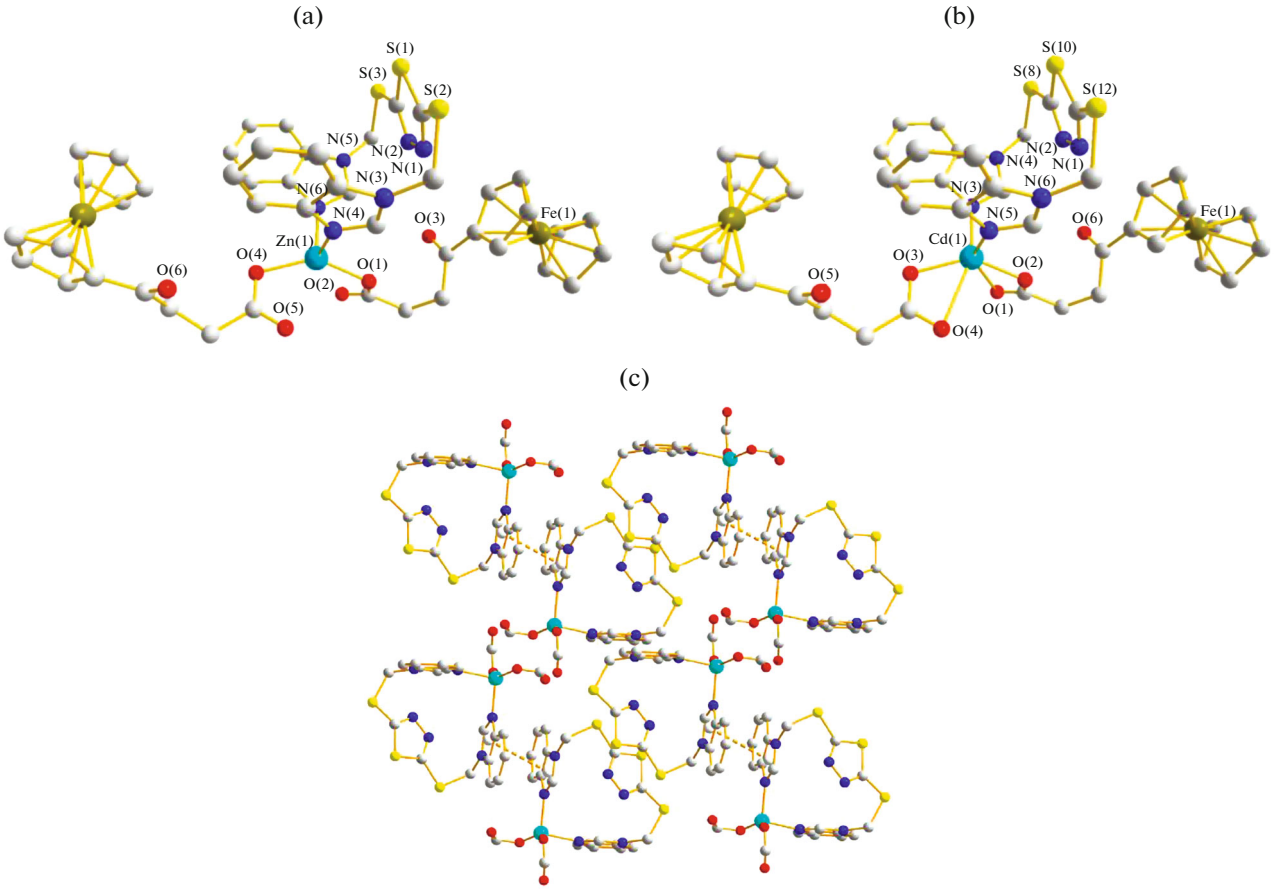

Fig. 3. The bowl-like structure of **III** (a); the mononuclear structure of and **IV** (b); the π···π interactions of **III** between two adjacent benzimidazole rings (c). Partial $FcCOC_2H_4COO^-$ units and hydrogen atoms are omitted for clarity.

ferrocene and benzene rings; and still the other is 2.95 Å (**III**) (3.11 Å for **IV**) (dihedral angel: 67.8° (**III**) (73.3° for **IV**); H/π-plane separation: 2.73 Å (**III**) (2.97 Å for **IV**)) between intramolecular benzimidazole and ferrocene rings. Such intramolecular or intermolecular interactions are essential in complexes **I**–**IV**, where they contribute significantly to molecular self-assembly processes.

TG analyses are performed to determine thermal stabilities of complexes **I**–**IV** (Fig. 4). The TG curve for **I** shows the initial weight loss in the temperature range of 30–137°C, which is due to the removal of free methanol molecule (obsd. 1.58%, calcd. 0.82%). Further weight loss indicates the decomposition of coordination framework, leading to compounds of ZnO + Fe_2O_3 as residue (obsd. 23.36%, calcd. 24.27%). The corresponding DSC curve clearly exhibits three strong exothermic peaks at 247, 469 and 549°C, respectively. For complex **II**, a gradual weight loss between 30 and 190°C is attributed to the release of one lattice water molecule (obsd. 2.00%, calcd. 2.02%). Hereafter, the host framework starts to decompose. The final residue of 25.11% is close to the calculated value of 26.88% based on ZnO + Fe_2O_3.

The thermal decomposition behavior of complex **III** is similar to that of **IV**. The TG curves of complexes **III** and **IV** both exhibit three continuous weight loss stages from 205–650°C (**III**) (210–630°C (**IV**)) corresponding to the decomposition of Bbbmd and $FcCOC_2H_4COO^-$ ligands. Finally, in complex **III**, a plateau region is observed from 650 to 750°C. There remain to be a brown fine crystalline powder of ZnO + Fe_2O_3 (obsd. 21.54%, calcd. 22.98%). In complex **IV**, the plateau region is between 630 to 750°C, the decomposition process is completed at 750°C giving brown fine crystalline powder CdO + Fe_2O_3 as the final decomposition product (obsd. 26.66%, calcd. 26.37%). In the DSC curve of **III**, there are two big exothermic peaks at 297 and 572°C and one strong endothermic peak at 201°C. In **IV**,

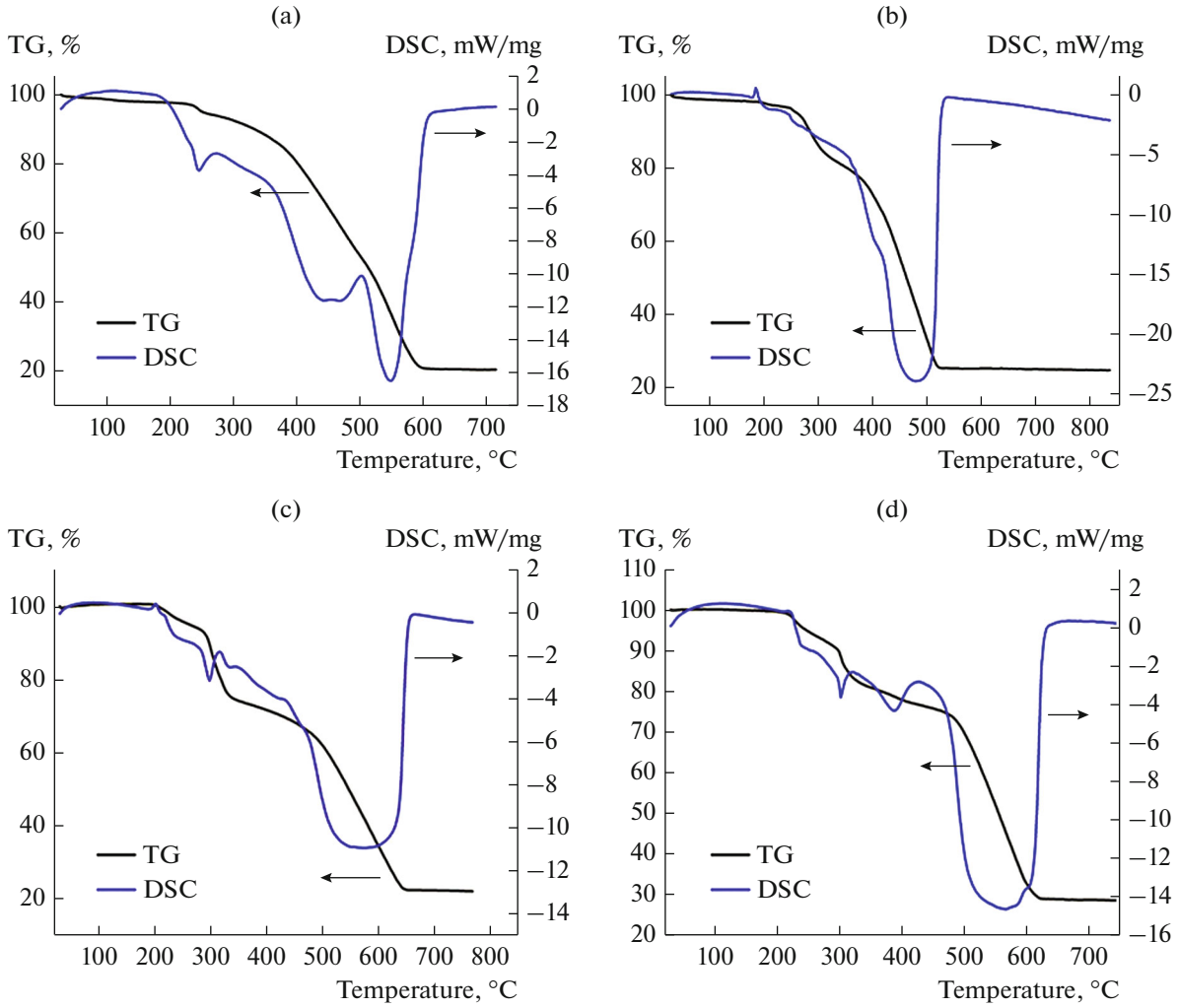

Fig. 4. The thermal decomposition curves of **I** (a), **II** (b), **III** (c), **IV** (d).

three main successive exothermic processes appear at 302, 388 and 566°C. There are slight differences in TG curves of complexes **III** and **IV** arised from different coordination modes of $FcCOC_2H_4COO^-$ that could influence their stabilities at high temperatures.

The electrochemical behavior of complexes **I**–**IV** and $FcCOC_2H_4COOH$ have been studied by cyclic voltammetry (Fig. 5a) and differential pulse voltammetry (Fig. 5b) in DMF solutions (~5.0×10^{-4} M total Fc concentrations) containing 0.1 M *n*-Bu_4NClO_4 as the supporting electrolyte. According to Fig. 5a, all those complexes exhibit an irreversible redox wave observed in several similar $FcCOC_2H_4COOH$ containing complexes [19]. As shown in Fig. 5b, all those complexes show a single peak with a half-wave potential ($E_{1/2}$ vs. *SCE*) at 0.760 V for **I**, 0.768 V for **II**, 0.740 V for **III**, 0.728 V for **IV**, and 0.716 V for the ligand in correspondence to redox processes of Fe(II)/Fe(III) couple electron-transfer process of ferrocenyl moieties [19, 31, 32].

FUNDING

We are thankful for financial support from National Natural Science Foundation of China (no. J1210060), Science and technology research program of Henan Province of China (nos. 162102210167, 172102210483), Key scientific research projects of Henan Province of China (no. 17A150020), Natural Science Foundation of Henan Province of China (no. 182300410216), National Undergraduate Innovation and entrepreneurship training project (no. 201810459007), College Science and Technology Innovation Team of Henan Province (no. 16IRTSTHN001) and

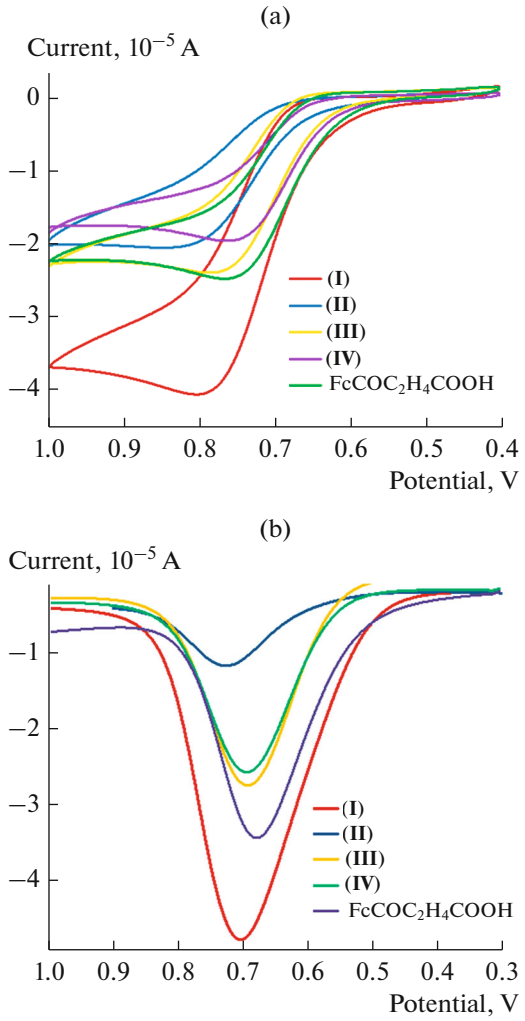

Fig. 5. Cyclic voltammograms (a) and differential pulse voltammograms (b) of complexes **I**–**IV** and $FcCOC_2H_4COOH$ (~5.0 × 10^{-4} M) in DMF solution containing *n*-Bu_4NClO_4 (0.10 M).

the Science & Technology Innovation Talent Plan of Henan Province (no. 174200510018).

REFERENCES

1. Castillo-Blum, S.E. and Barba-Behrens, N., *Coord. Chem. Rev.*, 2000, vol. 196, p. 3.
2. Liu, C.S., Wang, J.J., Yan, L.F., et al., *Inorg. Chem.*, 2007, vol. 46, p. 6299.
3. Yu, T.T., Wang, S.M., Li, X.M., et al., *CrystEngComm*, 2015, vol. 18, p. 1350.
4. Blake, A.J., Champness, N.R., Hubberstey, P., et al., *Coord. Chem. Rev.*, 1999, vol. 183, p. 117.
5. Li, J.P., Li, B.J., Pan, M.T., et al., *Cryst. Growth Des.*, 2017, vol. 17, p. 2975.
6. Togni, A. and Hayashi, T., *Ferrocenes: Homogeneous Catalysis, Organic Synthesis, Materials Science*, New York: VCH, 1995.
7. *Metallocenes*, Togni, A. and Haltermann, R.L., Eds., New York: Wiley-VCH, 1998.
8. Osborne, A.G., Silva, M.W.D., Hursthouse, M.B., et al., *J. Organomet. Chem.*, 1996, vol. 516, p. 167.
9. Osella, D., Ferrali, M., Zanello, P., et al., *Inorg. Chim. Acta*, 2000, vol. 306, p. 42.
10. Cheng, J.J., Wang, S.M., Shi, Z., et al., *Inorg. Chim. Acta*, 2016, vol. 453, p. 86.
11. Yaghi, O.M., Davis, C.E., Li, G.M., et al., *J. Am. Chem. Soc.*, 1997, vol. 119, p. 2861.
12. Duan, Y.Q., Huang, J.H., Liu, S.C., et al., *Inorg. Chem. Commun.*, 2017, vol. 81, p. 47.
13. Hao, Y.P., Yue, C.P., Jin, B.N., et al., *Polyhedron*, 2017, vol. 139, p. 296.
14. Zhang, Q.K., Yue, C.P., Zhang, Y., et al., *Inorg. Chim. Acta*, 2018, vol. 473, p. 112.
15. Li, J.P., Li, X.F., Lu, H.J., et al., *Inorg. Chim. Acta*, 2012, vol. 384, p. 163.
16. Withersby, M.A., Black, A.J., Champness, N.R., et al., *Angew. Chem. Int. Ed.*, 1997, vol. 36, p. 2327.
17. Bartholomew, G.P. and Bazan, G.C., *Acc. Chem. Res.*, 2001, vol. 34, p. 30.
18. Hoeben, F.J.M., Jonkheijm, P., and Meijer, P.W., *Chem. Rev.*, 2005, vol. 105, p. 1491.
19. Zhou, C.L., Wang, S.M., Liu, S.N., et al., *J. Mol. Struct.*, 2016, vol. 1118, p. 139.
20. Rinehart, K.L., Curby, R.J., and Sokol, P.E., *J. Am. Chem. Soc.*, 1957, vol. 79, p. 3420.
21. Hoskins, B.F., Robson, R., and Slizys, D.A., *J. Am. Chem. Soc.*, 1997, vol. 119, p. 2952.
22. Sheldrick, G.M., *Acta Crystallogr., Sect. A: Found. Crystallogr.*, 2008, vol. 64, p. 112.
23. Chen, D.M., Zhang, N.N., Liu, C.S., et al., *Appl. Mater. Interfaces*, 2017, vol. 9, p. 24671.
24. Sun, H., Zhang, Y.N., Si, X.Q., et al., *Synth. React. Inorg. Met.-Org. Nano-Met. Chem.*, 2013, vol. 43, p. 739.
25. Barquin, M., Cancela, J., Garmendia, M.J.G., et al., *Polyhedron*, 1998, vol. 17, p. 2373.
26. Li, Y.L., Wang, J., Shi, B.B., et al., *Supramol. Chem.*, 2015, vols. 7–8, p. 640.
27. Thaimattam, R., Xue, F., Sarma, J.A.R.P., et al., *J. Am. Chem. Soc.*, 2001, vol. 123, p. 4432.
28. Desiraju, G.R. and Steiner, T., Oxford: Oxford Univ., 1999.
29. Black, A.J., Baum, G., Champness, N.R., et al., *J. Chem. Soc., Dalton. Trans.*, 2000, vol. 23, p. 4285.
30. Hu, T.L., Li, J.R., Liu, C.S., et al., *Inorg. Chem.*, 2006, vol. 45, p. 162.
31. Zheng, G.L., Ma, J.F., Su, Z.M., et al., *Angew. Chem. Int. Ed.*, 2004, vol. 43, p. 2409.
32. Barranco, E.M., Crespo, O., Gimeno, M.C., et al., *Dalton. Trans.*, 2001, p. 2523.